Available online at www.sciencedirect.com

SciVerse ScienceDirect

Ceramics International 39 (2013) 4383–4390

CERAMICS INTERNATIONAL

www.elsevier.com/locate/ceramint

Structural, morphological, and gas response properties of citrate gel synthesized nanocrystalline ZnO and $Zn_{0.9}Cd_{0.1}O$ materials

J.Y. Patil[a], A.V. Rajgure[a], L.K. Bagal[a], R.C. Pawar[b], I.S. Mulla[c], S.S. Suryavanshi[a,*]

[a]School of Physical Sciences, Solapur University, Solapur 413255, India
[b]Department of Materials Engineering, Hanyang University, Ansan 426-791, South Korea
[c]Emeritus Scientist (CSIR), Centre for Materials for Electronic Technology(C-MET) Pune 411 008, India

Received 25 June 2012; received in revised form 23 October 2012; accepted 9 November 2012
Available online 16 November 2012

Abstract

ZnO and $Zn_{0.9}Cd_{0.1}O$ powders were synthesized using a citrate gel combustion method. The citrate gel combustion process provides homogeneous and phase pure nanocrystalline powders through a single step exothermic reaction. The pellets of ZnO and $Zn_{0.9}Cd_{0.1}O$ were sintered at 600 °C for 6 h and further used to study their structural, morphological, and gas response properties. The XRD and TEM study reveals formation of nanocrystaline powders for both compositions. The gas sensing properties of the pelletized sensor materials were studied at operating temperatures from 200 to 450 °C. It has been observed that gas response considerably depends upon the operating temperature and test gas species. The operating temperature of the ZnO sensor significantly decreased with addition of cadmium. The reproducibility and stability study of $Zn_{0.9}Cd_{0.1}O$ confirmed its candidature for acetone sensor related applications.

Keywords: Semiconductor; Chemical synthesis; TEM; SEM

1. Introduction

Extensive research is going on in order to detect and monitor harmful gases and more importantly in understanding the gas response properties. In this regard, metal oxide semiconductor (MOS) gas sensors have attracted great attention because of increasing concern over safety in residential areas and industrial complexes. They have been used widely for the detection of inflammable and toxic gases [1–7] due to their low cost and real-time detection ability. However, pure MOS materials relatively have poor sensing performance, and it can be enhanced by doping with other elements [8–11]. Literature study reveals that, the dopants could mainly be classified into two categories: (a) in the crystal lattice substituting the parent metal atom and (b) creating other metal oxide phases besides the original one. In both the ways, dopants can successfully enhance the gas sensing property of MOS. The nanosized gas sensor with compatible size and ease of operation is an important requisite. The sensing mechanism is a surface phenomenon and is based on the reaction between adsorbed oxygen species on the surface of semiconductor oxide and the gas molecules to be detected. The interaction between adsorbed oxygen species and the test gas induces change in electric properties due to transport of charge carriers to conduction band of base material. The response of the gas sensing material depends on various factors such as dopants, grain size, surface states, amount of adsorbed oxygen, and its activation energy. The effect of dopant on grain size and gas sensor behavior has been extensively studied [12,13]. The nanocrystalline ZnO in bulk and thin film form [14] have been widely studied for various applications like gas sensors, solar cells, varistor, and optoelectronic devices. The ZnO has three key advantages; firstly, it is semiconductor with direct wide band gap of 3.37 eV and has a large excitation binding energy. Secondly, its resistivity can be varied through a large range (10^{-3}–10^{5} Ω cm). It possesses excellent stability, high sensitivity, low fabrication complexity, and moderate operating temperatures, which are ideal properties for a gas sensing material. The physical and chemical properties

*Corresponding author. Tel.: +91 217 2744770.
E-mail address: sssuryavanshi@rediffmail.com (S.S. Suryavanshi).

0272-8842/$ - see front matter © 2012 Elsevier Ltd and Techna Group S.r.l. All rights reserved.
http://dx.doi.org/10.1016/j.ceramint.2012.11.026

of ZnO can be easily tailored by using suitable dopant material. Wan et al. [15] had studied the humidity sensing properties of Cd-doped ZnO nanowires, which were synthesized by simple thermal co-evaporation method. The Cd doped ZnO nanowires showed extremely high and fast response to the humidity pulse at room temperature. Ning Han et al. [16] reported the co-precipitation synthesis of Sn doped ZnO in which 10 mol% CdO activated 2.2 mol% Sn-doped ZnO shows the highest formaldehyde response at lower working temperature of 200 °C than 400 °C of pure ZnO. Bodade et al. [17] reported the polymerized complex synthesis of ZnO:-TiO_2:10 mol% CdO system using pressure bomb in which the ZnO:TiO_2:10 mol% CdO exhibits good response toward H_2S at lower operating temperature of 225 °C.

Various methods have been proposed for the synthesis of nanocrystalline ZnO which includes spray pyrolysis [18,14], sputtering method [19], co-precipitation [20], microemulsion [21], hydrothermal method [22–24], sol gel [25], and citrate gel combustion method [26]. The low temperature combustion methods [27–29] have proven to be very useful for the synthesis of nanocrystalline ZnO powders. These chemical synthesis methods provide significant advantages like good stoichiometric control, production of ultra fine particles with narrow size distribution in relatively short processing time. To the best of our knowledge, the gas sensing properties of ZnO and $Zn_{0.9}Cd_{0.1}O$ prepared by citrate gel combustion method have not been reported. The present work deals with the citrate gel combustion synthesis of ZnO and $Zn_{0.9}Cd_{0.1}O$ and studies on their structural, morphological, and reducing gas response properties.

2. Experimental details

2.1. Synthesis of ZnO and $Zn_{0.9}Cd_{0.1}O$ powders

The ZnO and $Zn_{0.9}Cd_{0.1}O$ powders were synthesized using the citrate gel combustion method. Analytical grade zinc nitrate hexahydrate ($Zn(NO_3)_2 \cdot 6H_2O$), cadmium nitrate hexahydrate ($Cd(NO_3)_2 \cdot 6H_2O$) and citric acid ($C_6H_8O_7 \cdot H_2O$) (purity 99.9%) were used as starting precursors. No further purification of the precursors was carried out. The metal nitrates and fuel were used in the stoichiometric ratio as per the propellant chemistry which is equal to 1:0.5 mol [28]. At this ratio, not only the rate of reaction but also the heat liberated per unit time are maximum. It is the ratio at which the oxygen content of oxidizer is completely reacted to oxidize or consume fuel completely and no external oxygen is required for reaction completion.

In a typical experiment the mixture containing the metal nitrates and citric acid was heated on a hot plate. Boiling the mixture resulted into a brown gaseous product which frothed, swelled, and got ignited. This exothermic reaction resulted into voluminous, fluffy nanocrystalline powders. This as synthesized powder was calcined at 500 °C for 2 h. The calcined powder was then made into pellets by applying pressure of 150 MPa using polyvinyl alcohol as a binder. Finally the pellets of ZnO and $Zn_{0.9}Cd_{0.1}O$ were sintered at 600 °C for 6 h in air and used further to study the structural, morphological, and gas response properties.

2.2. Characterization of the material

The X-ray diffraction (XRD) pattern of the samples were obtained on BRUKER AXS D8-Advanced X-ray diffractometer using Cu-Kα ($\lambda = 1.5405$ Å) radiation at 2θ values between 20° and 80°. The morphological features of the product were imaged using scanning electron microscope instrument (Model JSM-6360). The transmission electron microscopic (TEM) analysis and selected area electron diffraction (SAED) were performed on the microscope equipped (Philips CM 200 FEG)with a field emission gun at an accelerating voltage of 200 kV, with a resolution of 0.24 nm.

The lattice parameters of the ZnO and $Zn_{0.9}Cd_{0.1}O$ were calculated using the formula for interplanar spacing. The average crystallite size, D, was calculated from the Scherrer formula:

$$D = (0.9\lambda)/(\beta \cos\theta), \tag{1}$$

where 'β' is the full width at half maximum(FWHM) for most intense (101) reflection, 'θ' the angle of reflection, and 'λ' the wavelength of X-ray radiation used.

The apparent density of the sintered sample was calculated by considering the cylindrical shape of the pellets and using the relation:

$$d = \frac{m}{V} = \frac{m}{\pi r^2} h \tag{2}$$

where 'm' is the mass, 'r' is the radius and 'h' is the thickness of the pellet. The theoretical density (d_x) was calculated from the equation [30]:

$$d_x = \frac{8M}{Na^3} \tag{3}$$

where, 'M' is the molecular weight, 'N' is Avogadro's number and 'a' is the lattice parameter). The % porosity was calculated from the relation:

$$P(\%) = \left(1 - \frac{d}{dx}\right) \times 100 \tag{4}$$

2.3. Gas response measurement

The sintered pellets were tested for gas response properties towards various reducing gases, viz. liquid petroleum gas (LPG), acetone (CH_3COCH_3), ethanol (C_2H_5OH), and ammonia (NH_3). The details of the gas sensing set up used to study the gas response measurement is reported elsewhere [31]. The temperature of the system was controlled from room temperature to 500 °C (±2 °C) and the two-probe dc measurement technique was used to measure the resistance of the sample in the presence of air and relevant

test gas. Conducting silver paste was used to make the ohmic contacts on the pellets. The pellet was mounted on two probe ceramic sample holder placed in the glass tube assembly which was inserted coaxially inside a tubular furnace. The dimensions of the pellets were kept constant for all the samples prepared for the gas response measurements. The sensor was heated with continuous air flow for 2 h before measurements in order to attain stable resistance value. The known amount of test gas was introduced in the glass tube assembly of 1 l volume so that their required parts per million (ppm) concentration is attained. The resistance of the pellet was measured as a function of time at different operating temperatures and concentrations of test gas. The sensor responses of ZnO and $Zn_{0.9}Cd_{0.1}O$ were investigated in the temperature range of 200–450 °C under identical experimental conditions. The performance of the sensor was confirmed through the repeatability and reproducibility experiments. For repeatability, two to three cycles of the gas response characteristics were performed for each composition. For reproducibility, the gas response performance of at least two to three samples of each composition was tested.

The response is defined as:

$$S(\%) = \frac{(R_a - R_g)}{R_a} \times 100 \quad (5)$$

where, R_a is the resistance of sensor in air and R_g the resistance in the presence of test gas.

3. Result and discussion

3.1. Structural characterization

The structural properties of the ZnO and $Zn_{0.9}Cd_{0.1}O$ samples were studied and the corresponding X-ray diffraction pattern is shown in Fig. 1. The XRD pattern of sintered compositions show the presence of (100), (002), (101), (102), (110), (103), (200), (112), (201), (004), and (202) diffraction peaks of hexagonal wurtzite structure ZnO, along with three very low intensity peaks corresponding to the CdO phase. The strong intensity and narrow width of the ZnO diffraction peaks indicate that the resulting products are of high crystallinity. The d values calculated for the diffraction peaks are in good agreement with those given in JCPD data card (79–2205) for ZnO. The relative intensity sequence of diffraction peaks is analogous to those given in the JCPD data confirming the random orientation of the powder crystallites.

The lattice parameters and crystallite size corresponding to as prepared and sintered samples are shown in Table 1. It is found that, the crystallite size increases after both sintering and cadmium doping. The ionic radius of Cd^{2+} ion (97 pm) is larger than that of Zn^{2+} ion (74 pm). When Zn^{2+} ion is partially substituted with Cd^{2+}, the crystal cell increases without changing the wurtzite structure. CdO also enhances the growth of crystal size; however the occurrence of low intensity peaks belonging to CdO may

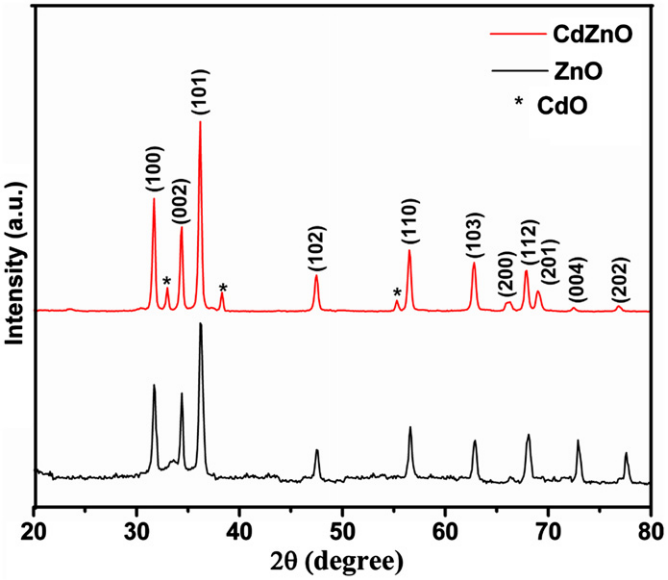

Fig. 1. X-ray diffraction pattern for ZnO and $Zn_{0.9}Cd_{0.1}O$ sintered at 600 °C for 6 h.

Table 1
Crystallite size and lattice parameter for ZnO and $Zn_{0.9}Cd_{0.1}O$ samples.

Name	Crystallite Size (nm)	Lattice parameter	
		a	c
As synthesized ZnO	20	3.256	5.214
Sintered ZnO	25	3.256	5.209
As synthesized $Zn_{0.9}Cd_{0.1}O$	28	3.250	5.206
Sintered $Zn_{0.9}Cd_{0.1}O$	33	3.255	5.221

be due to partial replacement of Zn^{2+} ions in the ZnO lattice by Cd^{2+} indicating that not all CdO was built into the ZnO lattice. It is thus confirmed that both ZnO and $Zn_{0.9}Cd_{0.1}O$ can be prepared by means of this citrate gel combustion method. The TEM and SAED images of the as synthesized ZnO and $Zn_{0.9}Cd_{0.1}O$ are presented in Fig. 2. It is vivid that the combustion method yielded hexagonal shaped nanoparticles with crystallite size in good agreement with that of XRD. As observed in XRD study the crystallite size of $Zn_{0.9}Cd_{0.1}O$ is higher than that of ZnO. The Selected Area Electron Diffraction (SAED) pattern shows the presence of rings corresponding to different planes of wurtzite ZnO as represented in XRD pattern.

3.2. Morphological study

The SEM images of the ZnO and $Zn_{0.9}Cd_{0.1}O$ sintered at 600 °C are shown in Fig. 3. SEM observation shows formation of highly porous surface for both the compositions which are attributed to the nanocrystalline powders used to make the pellets. The porosity for ZnO and $Zn_{0.9}Cd_{0.1}O$ samples were 51 and 50% respectively. There

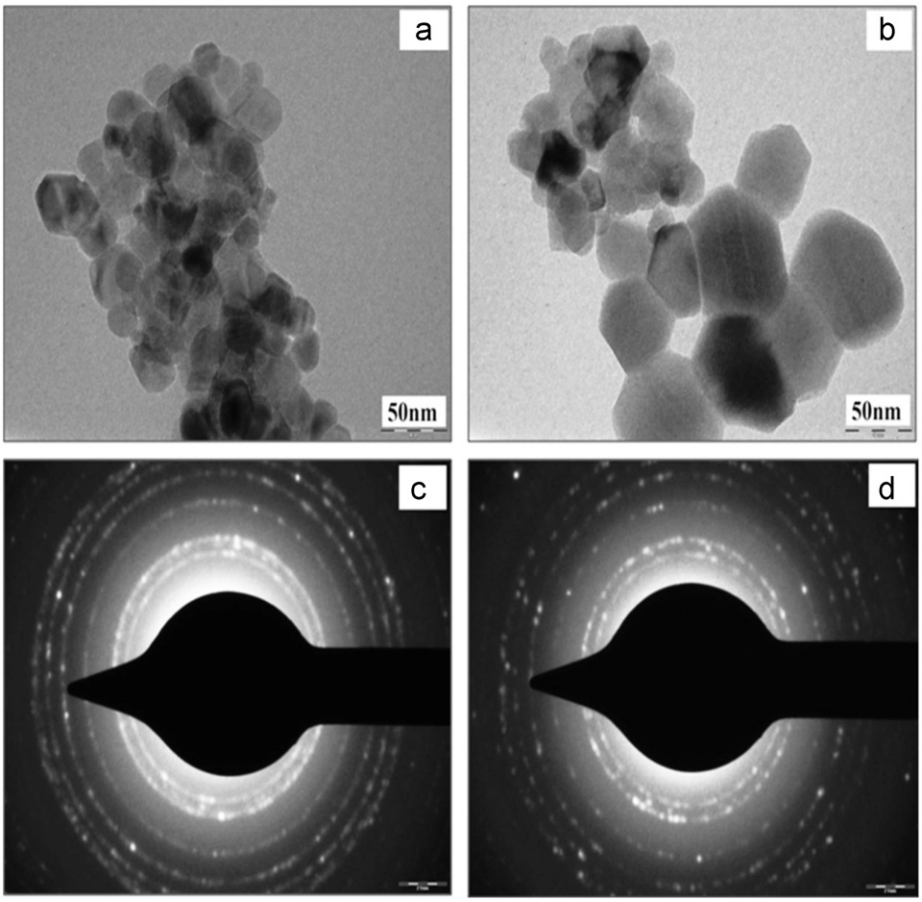

Fig. 2. TEM and SAED images of as synthesized (a) ZnO and (b) $Zn_{0.9}Cd_{0.1}O$.

is no much variation in porosity with Cd doping; however both samples possessed significantly high porosity which is mainly due to the low sintering temperature in the present case. The nanocrystallinity together with the high porosity can enhance the gas response of the material because more gas adsorption sites are available due to the increased surface area.

3.3. Gas response properties

The gas response measurements were taken during cooling of the sample after heating the pelletized samples at high temperature for sufficient time for gaining stability, thereby securing a good reproducibility of the response characteristics.

3.3.1. Response characteristics of ZnO

Fig. 4 depicts the response of ZnO sensor towards different test gases as a function of operating temperature. The sensor shows maximum response to each gas corresponding to a particular temperature. It is seen that the ZnO exhibit a typical n-type semiconducting behavior as there is a drop in resistance of the sensor when it is exposed to reducing gas. The LPG response of sensor was found to be increased with operating temperature, however the response to acetone and ethanol vapors was found to get saturated or decreased beyond a particular temperature. The sensor exhibits maximum response of 85, 94, and 83% towards LPG, acetone, and ethanol at operating temperatures of 450, 375, and 375 °C respectively. The response increases with temperature because thermal energy helps the reactions involved to overcome their respective activation energy barriers. However, at high operating temperature, the adsorbed oxygen species at the sensing sites on the sensor surface will be diminished and less available to react with test gases, thereby limiting the sensor response. The response of ZnO at optimized temperature as a function of concentration of test gas is shown in Fig. 5. The response was found to be increased with concentration of test gas.

3.3.2. Response characteristics of $Zn_{0.9}Cd_{0.1}O$

The response of $Zn_{0.9}Cd_{0.1}O$ sensor sintered at 600 °C is depicted in Fig. 6. From figure, it is obvious that the operating temperature for acetone and ethanol has significantly decreased as compared to ZnO. The response to acetone, ethanol, and LPG increased marginally; however for ammonia it has reduced. The sensor shows a wide operating temperature range for acetone giving almost constant response over that range. The sensor shows the highest response of 86, 96, and 91%, towards LPG,

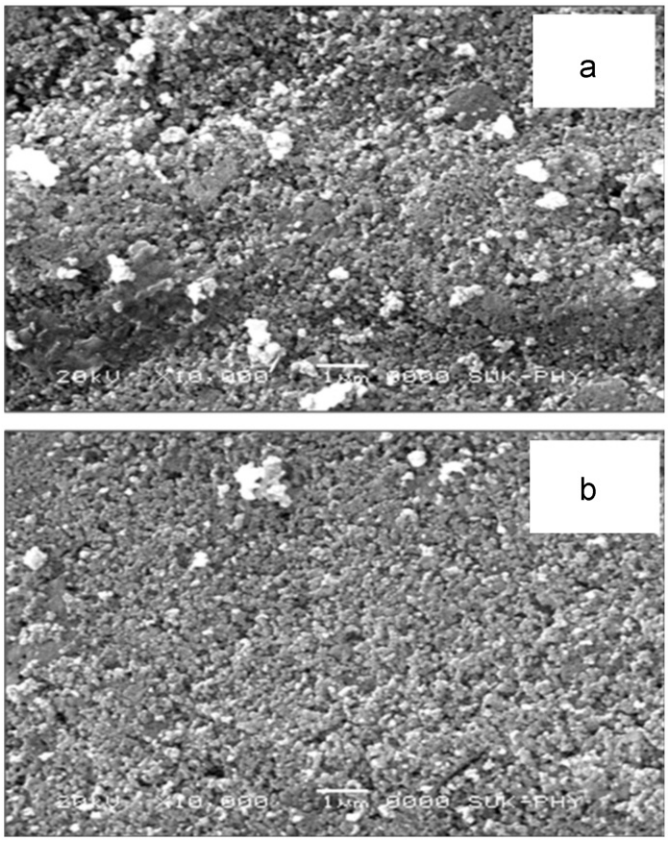

Fig. 3. SEM images of (a) ZnO and (b) $Zn_{0.9}Cd_{0.1}O$ sintered at 600 °C for 6 h.

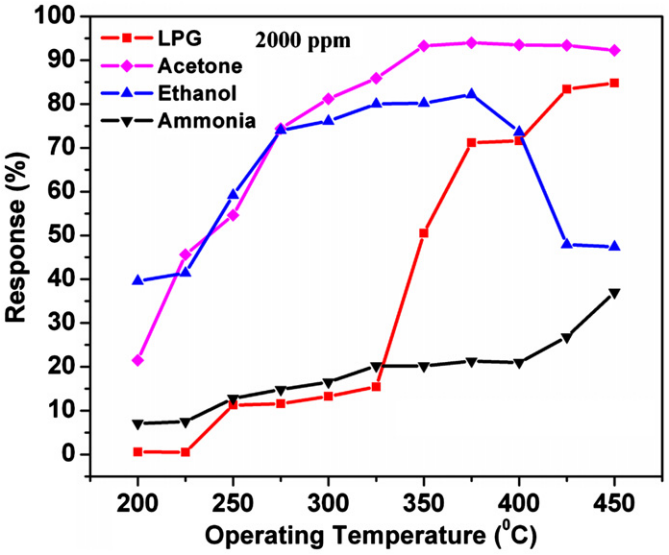

Fig. 4. The variation of response of ZnO with operating temperature.

acetone, and ethanol at operating temperatures of 400, 275, and 300 °C respectively. The response as a function of concentration of test gases for $Zn_{0.9}Cd_{0.1}O$ at their optimum operating temperature is given in Fig. 7. The response was found to be increased with concentration of

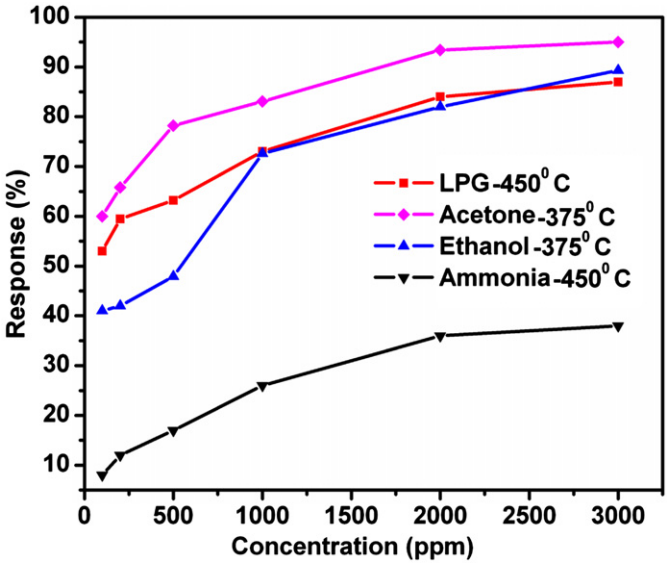

Fig. 5. The variation of response of ZnO with concentration of the test gases.

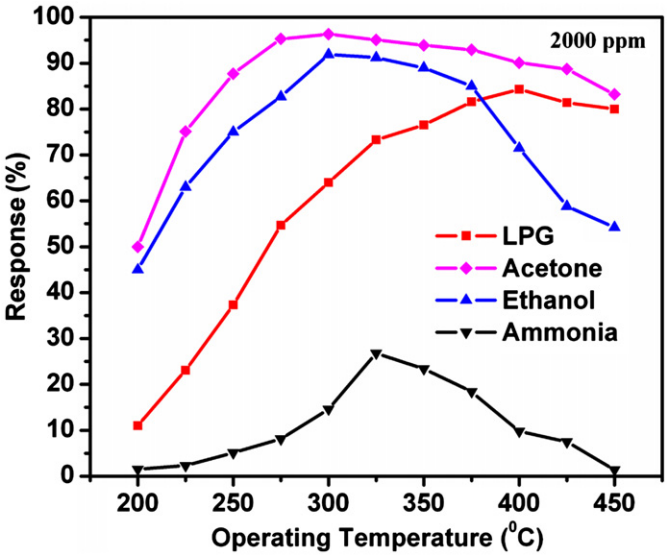

Fig. 6. The response of $Cd_{0.1}Zn_{0.9}O$ as a function of operating temperature.

test gas similar to that of ZnO. The response of a sensor depends on removal of adsorbed oxygen molecules by reaction with a target gas and generation of electrons. For a small concentration of gas, exposed on a fixed surface area of a sample, there is a lower coverage of gas molecules on the surface and hence lower surface reaction occurs. An increase in gas concentration increases the surface reaction due to a larger surface coverage resulting into the higher response. In general sensor response (S) in % versus concentration (C) in ppm of target gas or vapor is represented by the empirical relation[32]: $S = A[C]^N + B$, where A and B are constants and C is the concentration of the target gas or vapor. N usually has value between

0.5 and 1.0, depending on the change of the surface species and the stoichiometry of the elementary reactions on the surface. As shown in Figs. 5 and 7 a curvilinear relationship between response and the test gas concentration is observed, indicating $N=0.5$ for all samples and test gases.

3.3.3. Acetone and ethanol sensing mechanism on the surface of ZnO and $Zn_{0.9}Cd_{0.1}O$

The gas sensing mechanism of ZnO and $Zn_{0.9}Cd_{0.1}O$ based sensors is the surface controlled process in which resistance change is controlled by the type and amount of chemisorbed oxygen ions on the surface. Depending upon the temperature and metal oxide surface, the atmospheric oxygen is chemisorbed on the sensor surface in different forms such as O_2^-, O^{2-}, and O^-; which are available for catalytic reactions with test gases. O_2^- is commonly chemisorbed at low temperatures and at high temperatures however O^- and O^{2-} are commonly chemisorbed, while O^{2-} disappears rapidly. At the operating temperature range of 200–400 °C, O^- is mostly available for reaction with test gas. Consequently, the chemical reaction underlying the acetone and ethanol vapor sensing in this study is given as [33–35]:

$$CH_3COCH_2 + 8O^- \rightarrow 3CO_2 + 3H_2O + 8e^- \quad (6)$$

$$CH_3CH_2OH + 6O^- \rightarrow 2CO_2 + 3H_2O + 6e^- \quad (7)$$

The adsorbed O^- on the sensor surface reacts with the acetone and ethanol yielding CO_2, H_2O and releasing electrons back to the conduction band of the material which contribute to the decrease in resistance of the sensor material.

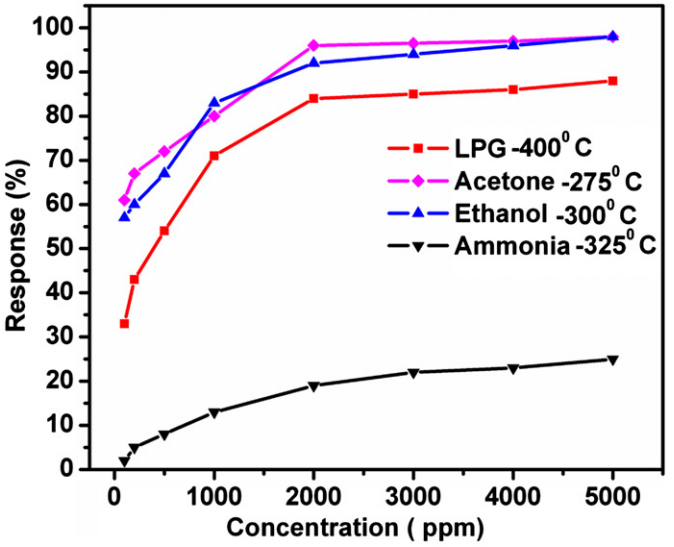

Fig. 7. The response of $Zn_{0.9}Cd_{0.1}O$ as a function of concentration of the test gases.

3.3.4. Response of ZnO and $Zn_{0.9}Cd_{0.1}O$ to 100 ppm of test gases

Fig. 8 compares the sensor response to each test gas for ZnO and $Zn_{0.9}Cd_{0.1}O$ at optimum operating temperatures for acetone. The ZnO sensor (Fig. 8(a)) exhibits response of 53, 60, and 41% towards LPG, acetone, and ethanol at the concentration of 100 ppm. However, the $Zn_{0.9}Cd_{0.1}O$ sensor (Fig. 8(b)) exhibits 33, 61, and 57% response towards LPG, acetone, and ethanol at 100 ppm. In case of $Zn_{0.9}Cd_{0.1}O$ the response towards acetone and ethanol is found to be increased while for LPG it has decreased. The $Zn_{0.9}Cd_{0.1}O$ sensor exhibits good selectivity and excellent response to acetone for 100 ppm concentration, at low operating temperature relative to pure ZnO.

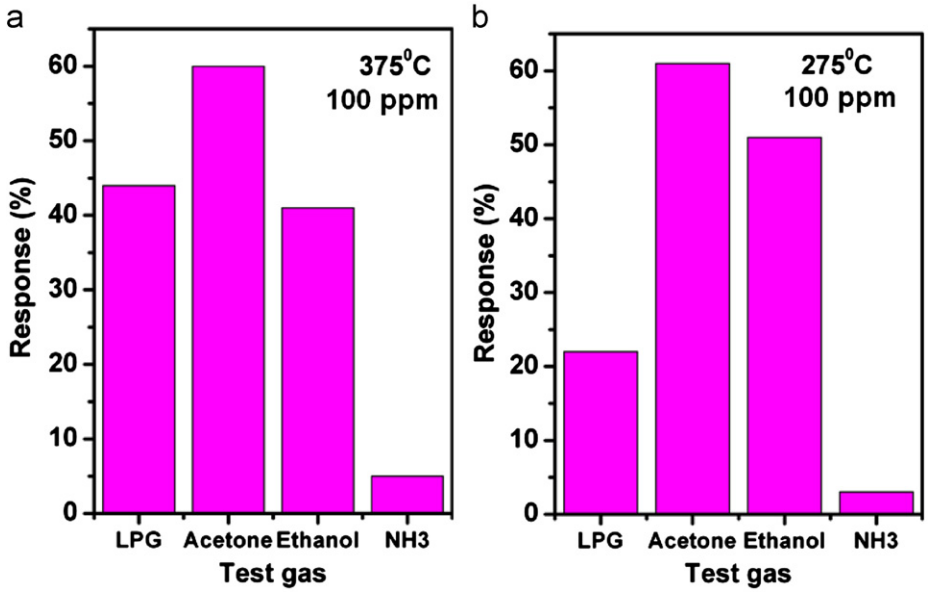

Fig. 8. The response of ZnO and $Zn_{0.9}Cd_{0.1}O$ to different test gases for 100 ppm concentration at the optimum operating temperatures for acetone.

3.3.5. Reproducibility and stability of $Cd_{0.1}Zn_{0.9}O$ sensor to acetone vapor at 275 °C

The sensor reliability is strongly dependent on the reproducibility and stability exhibited by the sensor material. The reproducibility and stability of the $Zn_{0.9}Cd_{0.1}O$ sensor sintered at 600 °C were measured by repeating the response measurement a number of times. Fig. 9 depicts the dynamic response transients for different samples of $Zn_{0.9}Cd_{0.1}O$ towards acetone. It is clear that the response of the material is almost constant confirming the reproducibility of sensor material. Stability is the consistence of the response of a sensor under continuous testing. The responses of the $Zn_{0.9}Cd_{0.1}O$ sensor towards acetone were measured on 15th, 30th, 45th and 60th days after the first measurement and it is shown in Fig. 10. It was found that after two months, the material performs 94% of its earlier performance confirming the stability and reliability of the sensor material for commercial application.

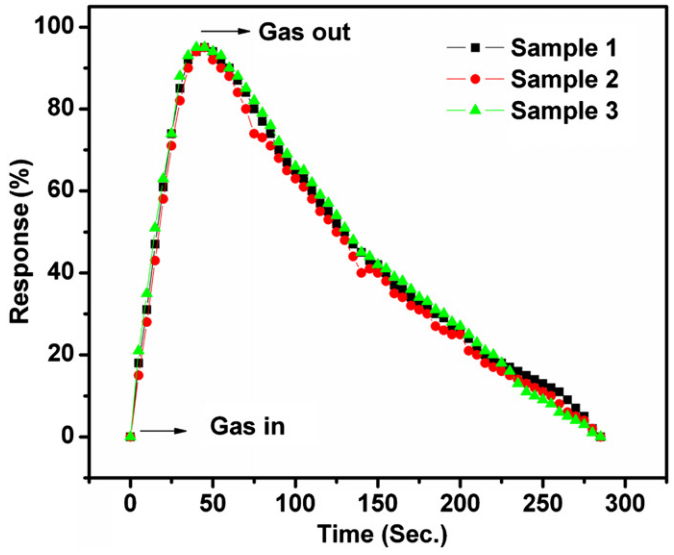

Fig. 9. Plot showing the reproducibility of $Zn_{0.9}Cd_{0.1}O$ to acetone at 275 °C.

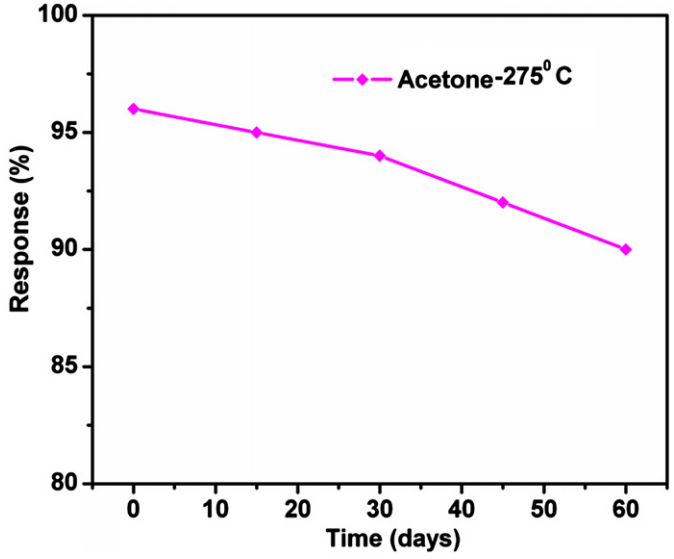

Fig. 10. Plot showing the stability of $Zn_{0.9}Cd_{0.1}O$ to acetone at 275 °C.

4. Conclusions

The ZnO and $Zn_{0.9}Cd_{0.1}O$ materials synthesized by citrate gel process yielded sensors with excellent response, fast response and recovery time at moderate operating temperatures. The results of this study also demonstrate the importance of Cd doping in ZnO gas sensors in decreasing the operating temperature of the sensor as an effect of reduction in crystallite size. The XRD and TEM study revealed the formation of nanocrystalline material using citrate gel combustion method. The nanocrystalline nature of the material found to play key role in gas sensing. From reproducibility and stability study we concluded that $Zn_{0.9}Cd_{0.1}O$ can stand as a reliable sensor element for acetone sensor related applications.

Declaration

The present work is original and informative and has not been published previously or it is not under consideration for publication elsewhere. All the authors are aware of its content and agreed to submit the paper in present form. There is not conflict of interest existed and if accepted, the article will not be published elsewhere in the same form, in any language, without the written consent of the publisher.

Acknowledgments

One of the authors J.Y. Patil acknowledges DAE-BRNS for the grant of JRF. I.S. Mulla, Emeritus Scientist is grateful to CSIR, Delhi. All the authors gratefully acknowledge DAE-BRNS, India for the financial support.

References

[1] K. Park, K.U. Jang, Response characteristics to reducing gases in $BaTiO_3$-based thick films, Journl of Alloys and Compounds 391 (2005) 123–128.
[2] K. Arshak, I. Gaidan, Development of a novel gas sensor based on oxide thick films, Materials Science and Engineering B 118 (2005) 44–49.
[3] L. Satyanarayana, K.M. Reddy, S.V. Manorama, Nanosized spinel $NiFe_2O_4$: a novel material for the detection of liquefied petroleum gas in air, Materials Chemistry and Physics 82 (2003) 21–26.
[4] S.I. Rembeza, E.S. Rambeza, T.V. Svistova, O.I. Borsiakova, Electrical resistivity ad gas response mechanisms of nanocrystalline SnO_2 films in a wide temperature range, Physica Status solidi (a) 179 (2000) 147.
[5] J.G. Partridge, M.R. Field, J.L. Peng, A.Z. Sadek, K. Kalantar-zadeh, J. Du Plessis, D.G. McCulloch, Nanostructured SnO_2 films prepared from evaporated Sn and their application as gas sensors, Nanotechnology 19 (2008) 125504 5pp.
[6] K. Mukherjee, S.B. Majumder, Analyses of conductance transients to address the selectivity issue of zinc ferrite gas sensors, Electrochemical and Solid State 13 (2010) J25–J27.

[7] S.K. Biswas, P. Pramanik, Studies on the gas sensing behaviour of nanosized $CuNb_2O_6$ towards ammonia, hydrogen and liquefied petroleum gas, Sensors and Actuators B 133 (2008) 449–455.
[8] J.H. Yu, G.M. Choi, Electrical and CO gas sensing properties of ZnO–SnO_2 composites, Sensors and Actuators B 52 (1998) 251–256.
[9] M. Zhao, X. Wang, L. Ning, J. Jia, X. Li, L. Cao, Electrospun Cu-doped ZnO nanofibers for H_2S sensing, Sensors and Actuators B 156 (2011) 588–592.
[10] N.J. Dayan, S.R. Sainkar, R.N. Karekar, R.C. Aiyer, Formulation and characterization of ZnO:Sb thick-film gas sensors, Thin Solid Films 325 (1998) 254–258.
[11] N. Han, Y. Tian, X. Wu, Y. Chen, Improving humidity selectivity in formaldehyde gas sensing by a two-sensor array made of Ga-doped ZnO, Sensors and Actuators B 138 (2009) 228–235.
[12] S.S. Badadhe, I.S. Mulla, Effect of aluminium doping on structural and gas sensing properties of zinc oxide thin films deposited by spray pyrolysis, Sensors and Actuators B 156 (2011) 943–948.
[13] S.C. Navale, I.S. Mulla, Photoluminescence and gas sensing study of nanostructured pure and Sn doped ZnO, Materials Science and Engineering C 29 (2009) 1317–1320.
[14] V.R. Shinde, T.P. Gujar, C.D. Lokhande, LPG sensing properties of ZnO films prepared by spray pyrolysis method: effect of molarity of precursor solution, Sensors and Actuators B 120 (2007) 551–559.
[15] Q. Wan, Q.H. Li, Y.J. Chen, T.H. Wang, X.L. He, X.G. Gao, J.P. Li, Positive temperature coefficient resistance and humidity sensing properties of Cd-doped ZnO nanowires, Applied Physics Letters 84 (2004) 3085–3087.
[16] N. Han, X. Wu, D. Zhang, G. Shen, H. Liu, Y. Chen, CdO activated Sn-doped ZnO for highly sensitive, selective and stable formaldehyde sensor, Sensors and Actuators B 152 (2011) 324–329.
[17] A.B. Bodade, A.M. Bende, G.N. Chaudhari, Synthesis and characterization of CdO-doped nanocrystalline ZnO:TiO_2-based H_2S gas sensor, Vacuum 82 (2008) 588–593.
[18] H. Tabet-Derrazn, N. Benramdane, D. Nacer, A. Bouzidi, M. Medles, Investigations on $Zn_xCd_{1-x}O$ thin films obtained by spray pyrolysis, Solar Energy Materials and Solar Cells 73 (2002) 249–259.
[19] D.W. Ma, Z.Z. Ye, J.Y. Huang, L.P. Zhu, B.H. Zhao, J.H. He, Effect of post-annealing treatments on the properties of $Zn_{1-x}Cd_xO$ films on glass substrates, Materials Science and Engineering B 111 (2004) 9–13.
[20] S.C. Navale, V. Ravi, D. Srinivas, I.S. Mulla, S.W. Gosavi, S.K. Kulkarni, EPR and DRS evidence for NO_2 sensing in Al-doped ZnO, Sensors and Actuators B 130 (2008) 668–673.
[21] C. Liangyuan, B. Shouli, Z. Guojun, L. Dianqing, C. Aifan, C.C. Liu, Synthesis of ZnO–SnO_2 nanocomposites by microemulsion and sensing properties for NO_2, Sensors and Actuators B 134 (2008) 360–366.
[22] B. Baruwati, D.K. Kumar, S.V. Manorama, Hydrothermal synthesis of highly crystalline ZnO nanoparticles: a competitive sensor for LPG and EtOH, Sensors and Actuators B 119 (2006) 676–682.
[23] Z. Bai, C. Xie, S. Zhang, L. Zhang, Q. Zhang, W. Xu, J. Xu, Microstructure and gas sensing properties of the ZnO thick film treated by hydrothermal method, Sensors and Actuators B 151 (2010) 107–113.
[24] X. Jiaqiang, C. Yuping, L. Yadong, S. Jianian, Gas sensing properties of ZnO nanorods prepared by hydrothermal method, Journal of Materials Science 40 (2005) 2919–2921.
[25] A. Erol, S. Okur, B. Comba, O. Mermer, M.C. Arikan, Humidity sensing properties of ZnO nanoparticles synthesized by sol–gel process, Sensors and Actuators B 139 (2009) 466–470.
[26] S.C. Navale, V. Ravi, I.S. Mulla, Investigations on Ru doped ZnO: strain calculations and gas sensing study, Sensors and Actuators B 145 (2010) 174–180.
[27] N.L. Tarwal, P.R. Jadhav, S.A. Vanalakar, S.S. Kalagi, R.C. Pawar, J.S. Shaikh, S.S. Mali, D.S. Dalavi, P.S. Shinde, P.S. Patil, Photoluminescence of zinc oxide nanopowder synthesized by a combustion method, Powder Technology 208 (2011) 185–188.
[28] S.K. Sharma, S.S. Pitale, M.M. Malik, R.N. Dubey, M.S. Qureshi, S. Ojha, Influence of fuel/oxidizer ratio on lattice parameters and morphology of combustion synthesized ZnO powders, Physica B—Condensed Matter 405 (2010) 866–874.
[29] S.K. Lathika Devi, K.S. Kumar, A. Balakrishnan, Rapid synthesis of pure and narrowly distributed Eu doped ZnO nanoparticles by solution combustion method, Materials Letters 65 (2011) 35–37.
[30] J. Smit, H.P.J. Wijn, Les Ferrites, Dunod, Paris, 1961.
[31] R.C. Pawar, J.S. Shaikh, A.V. Moholkar, S.M. Pawar, J.H. Kim, J.Y. Patil, S.S. Suryavanshi, P.S. Patil, Surfactant assisted low temperature synthesis of nanocrystalline ZnO and its gas sensing properties, Sensors and Actuators B 151 (2010) 212–218.
[32] Zhixue Wang, Lei Liu, Synthesis and ethanol sensing properties of Fe-doped SnO_2 nanofibers, Materials Letters 63 (2009) 917–919.
[33] P.A. Murade, V.S. Sangawar, G.N. Chaudhari, V.D. Kapse, A.U. Bajpeyee, Acetone gas-sensing performance of Sr-doped nanostructured $LaFeO_3$ semiconductor prepared by citrate sol–gel route, Current Applied Physics 11 (2011) 451–456.
[34] A.S. Kamble, R.C. Pawar, J.Y. Patil, S.S. Suryavanshi, P.S. Patil, From nanowires to cubes of CdO: ethanol gas response, Journal of Alloys and Compounds 509 (2011) 1035–1039.
[35] Z. Yang, Y. Huang, G. Chen, Z. Guo, S. Cheng, S. Huang, Ethanol gas sensor based on Al-doped ZnO nanomaterial with many gas diffusing channels, Sensors and Actuators B 140 (2009) 549–556.